Research Paper

Evaluation of the Effects of Spinel Ferrite Nanoparticles on the Composition of Normal Human Blood Serum

MOHAMMED MOULAY[1,2,3,4]*, MOHAMMED ALAMRI[5], STEVE HARAKEH[1,2], AFNAN ALQADIRI[3], RAED ALAZHAR[6], ALI ZARI[3] AND SALEH ALKARIM[1,3]

Embryonic Stem Cell Research Unit, [1]King Fahd Medical Research Center, [2]Department of Medical Laboratory Sciences, Faculty of Applied Medical Sciences, [3]Department of Biological Sciences, Faculty of Science, King Abdulaziz University, Jeddah 21589 Saudi Arabia, [4]Department of Biology, Abdelhamid bin Badis University, Mostaganem 27000, Algeria, [5]Ibn Sina National College for Medical Studies, Jeddah 22421, [6]Urology Department, King Abdulaziz Hospital, King Abdulaziz University, Jeddah 21589, Saudi Arabia

Magnetic ferrite-based nanoparticles have recently emerged as a promising alternative choice for the treatment of different types of cancer. Magnetic ferrite-based nanoparticles have already been used in diagnosis of various diseases and as a drug delivery vehicle. In this study, spinel ferrite nanoparticles were prepared using a hydrothermal approach which is a simple and cost-effective technique. Spinel ferrite nanoparticles were prepared from a variety of divalent metals including nickel, zinc, copper and cobalt. The impact of these nanoparticles on the composition of human blood serum was evaluated *in vitro*. Fourier-transform infrared and ultraviolet-visible absorption spectroscopies were used to examine the blood serum. According to the findings, all of the magnetic ferrite-based nanoparticles studies showed protein corona formation. The development of corona protein was due to the affinity of magnetic ferrite-based nanoparticles to interact with protein and size independent. The magnetic ferrite-based nanoparticles had no effect on the amino acid makeup of the serum. The magnetic ferrite-based nanoparticles exerted their efficacy by releasing a small amount of metal oxides into the serum. According to our findings, zinc ferrite was the most suited spinel ferrite nanoparticles to be evaluated further for their possible application in nanomedicine.

Key words: Nanomedicine, nanotechnology, human serum blood, spinal ferrite nanoparticles, protein corona

During the last decade, a considerable number of publications have focused on Nanoparticles (NPs) and their contribution in the field of nanomedicine development[1-10]. Magnetic Ferrite-Based Nanoparticles (MFNPs) have emerged as a novel material with potential applications in the fields of drug delivery, imaging, nanodiagnostic and therapy.

The most commonly used method to administer these NPs is intravenous injection. Consequently, these NPs can be in contact with human blood, which may affect different physiological processes in the human body. It can have a beneficial or therapeutic effect or may cause toxicity. Therefore, this study was undertaken with the objective of evaluating the effects of these NPs on the human blood and its components.

Due to its hydrophobicity, biocompatibility and biodegradability, albumin is the most abundant protein in the plasma and can be used to functionalize NPs and contribute to the drug delivery system due to its hydrophobicity[11]. Most of the albumin-associated drugs are carried in the blood stream. It has been demonstrated that when the NP's are in contact with the blood, they are spontaneously surrounded by proteins forming the protein-corona complex[12]. These corona proteins may have various effects on protein structure and functions, which are important in drug delivery and could cause toxicity too[10,13]. Therefore, the protein corona formation mechanism and its application have become an important research topic lately for nanomedicine development[8,14].

Several studies have found that the composition and size of the NPs, as well as the pH of the medium, can have a significant impact on protein adsorption[15,16]. The protein composition forming the corona depends on various parameters, namely the physicochemical

***Address for correspondence**
E-mail: mmoulay@kau.edu.sa

properties of the NP i.e. composition, shape, size, surface charge, hydrophobicity or hydrophilicity and the properties of the surrounding medium, i.e. protein source, temperature, pH and incubation time[17-19]. An intriguing feature of protein corona is that it varies among normal people and diseased individuals. Corbo *et al.*[20] have outlined these characteristics and introduced the concept of a personalized protein corona.

Several studies have reported the interaction of NPs (mostly metallic ones) with human blood serum. Chantada-Vazquez *et al.*[21] analyzed the proteomics of the corona formed on Gold (Au), Silver (Ag) and Platinum (Pt) NPs and concluded that the protein corona formation depends on the NPs composition and size. They also observed lower protein absorption by smaller NP. In another study, the same research group (Chantad-Vasquez *et al.*[21]) reported on the affinity of protein to Au, Ag and Iron (Fe).

In addition, the corona protein has also been reported to functionalize Silicon Dioxide (SiO_2) NPs for drug delivery[14]. Choimet *et al.*[7] investigated the interaction of apatite colloidal (phosphate and calcium compound) NPs with human blood components, finding that the surface charge was relatively inert.

Due to their magnetic properties and small size, Fe-based NPs are potential candidates for biomedical applications in magnetic resonance imaging[22,23], drug delivery[5] and magnetic hyperthermia[24]. Angglova *et al*. have studied the nano-colloids of Ferric Oxyhydroxide FeO(OH) functionalization by human serum albumin to produce an hematocompatible hybrid albumin entrapped FeO(OH) NPs. Martinez-Rodriguez *et al*.[13] examined the toxicity of Zinc (Zn) and Nickel Ferrite ($NiFe_2O_4$) NPs in peripheral blood mononuclear cells[25].

Gandhi *et al*. investigated the interaction of bovine serum albumin with Manganese Ferrite ($MnFe_2O_4$) NPs. They observed their biocompatibility and the amide bonds shift following the corona protein formation[26]. Most studies are concentrated on the formed protein coronas properties[4,12,14,21,27-30] and the NP's protein functionalization[31,32] while to the best of our knowledge, the effect of ferrite based MFNPs on human blood serum has not yet been investigated.

Herein, we investigated the effects of spinel ferrite NPs prepared with various divalent metals such as Ni, Cobalt (Co), Copper (Cu) and Zn, and their interactions with human blood serum.

MATERIALS AND METHODS

Synthesis of ferrite NPs:

Spinel ferrite NPs were prepared by the hydrothermal method. 0.1 M solution was prepared by dissolving two precursors $FeCl_3$ and metallic chloride (i.e. $NiCl_2$, $CuCl_2$, $CoCl_2$ and $ZnCl_2$) as sources of Fe, Ni, Cu, Co and Zn elements, respectively, in distilled water. The starting solution was magnetically stirred to obtain a transparent and homogeneous solution. The atomic ratio of the two metals was 75 % Fe and 25 % M (M=Zn, Co, Cu and Ni according to the studied metal). After that, 2 ml of ammonia were added to the solution in order to control the pH of the solution. The obtained mixture of 50 ml was heated in an autoclave at 200° for 6 h. The harvested powder was washed several times with mixture of ethanol and water and dried at 60° for 1 h in an open oven. The powder is then calcinated at 500° for 2 h in a temperature- regulated oven.

Powder characterizations techniques:

The powder structure was examined by the X-Ray Diffraction technique (XRD, D8 Advance, Brucker, Germany) operating at 40 kV and 40 mA with Copper K alpha (Cu kα) radiation (Lambda (λ)=0.154056 nm). The scanning was done in the angle range of 2θ from 20° to 80°.

The nanopowder morphology was studied by a field emission scanning electron microscope (JSM-7600F JEOL) and a transmission electron microscope operating at 200 kV (Type JEOL JSM-200F atomic resolution microscopy, Japan).

Serum sample preparation:

The serum was isolated from the blood of a voluntary individual in very healthy conditions. The blood sample was left at room temperature for 30 min to produce a blood clot. This clot was removed by centrifuging it at 12 000 rpm for 10 min at 4°. In 200 l of serum, 10 g of each ferrite nanopowder were mixed separately. In order to ensure the NPs come in contact with serum and to avoid their agglomeration, the mixture was shaken for 90 min at room temperature. After that, the mixture was stored overnight in the fridge at 4°. The supernatant was decanted in a new tube and used for further analysis *via* Fourier Transform Infrared (FTIR) spectroscopy using a Nicolet iS10 (Thermo Fisher Scientific Co, Waltham, Massachusetts, United States of America (USA)) in the interval of 400 to 4000 cm^{-1} using the

Attenuated Total Reflectance (ATR) and Ultraviolet (UV)-Visible absorption spectrophotometry using a Biotech Co, Winooski, Vermont, USA spectrophotometer in the wavelength range of 200-800 nm. The FTIR measurements were done on a 1 µl droplet of each solution. The serum without contact with nanopowder was used as a negative reference.

RESULTS AND DISCUSSION

Fig. 1 shows the XRD pattern of the pure ferrite and the synthetized hematite and spinel ferrite NPs using various divalent metals. The hematite (Fe_2O_3) pattern was composed of several diffraction peaks located at the following angles: 24.15°, 33.15°, 35.65°, 40.90°, 49.45°, 54.05°, 62.45° and 64.05°. These peaks are assigned respectively to the planes according to Joint Committee on Powder Diffraction Standards (JCPDS) card no 33-0664, (012), (104), (110), (113), (024), (116), (214) and (300) of the α-Fe2O3 rhombohedrally centered hexagonal hematite phase. The diffraction pattern of $NiFe_2O_4$ consisted of several peaks located at 30.2°, 35.6°, 37.3°, 43.3°, 53.8°, 57.3° and 63.0° assigned to the diffraction planes (220), (311), (222), (400), (422), (511) and (440) of the spinel ferrite phase (JCPDS: 01-074-2081). In addition, the powder prepared with Zn, Co and Cu divalent metal were a mixture of hematite and the spinel phase of $ZnFe_2O_4$, Cobalt Ferrite ($CoFe_2O_4$) and Copper Ferrite ($CoFe_2O_4$). No additional peaks of the second phase were observed in the XRD pattern, showing that the prepared ferrite is composed of single spinel phases.

Fig. 2 shows the Scanning Electron Microscopy (SEM) and Transmission Electron Microscopy (TEM) images of different MFNPs. From these images, it is quite clear that the prepared nano powders are mainly composed of agglomeration spherical grains with uniform size. As shown in Table 1, the grain size of Fe_2O_3 was found to be around 1200 nm. However, the grain size of powder prepared with Cu, Zn and Co exhibits larger grains, while $NiFe_2O_4$ was found to have lowest grain size of 56 nm.

The FTIR absorbance spectra of different samples before and after NPs treatment are depicted in fig. 3. The spectra of all samples are composed mainly of three peaks, which are characteristics of human blood serum. The latter is a complex medium containing a vast array of biomolecules, including over 20 000 protein varieties.

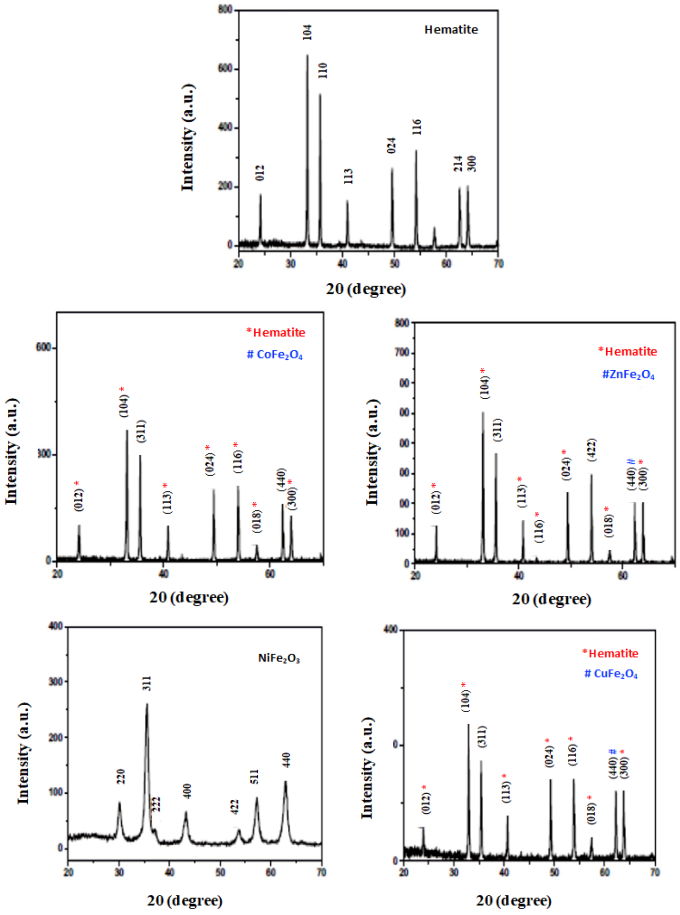

Fig. 1: XRD patterns of the different synthetized MFNPs

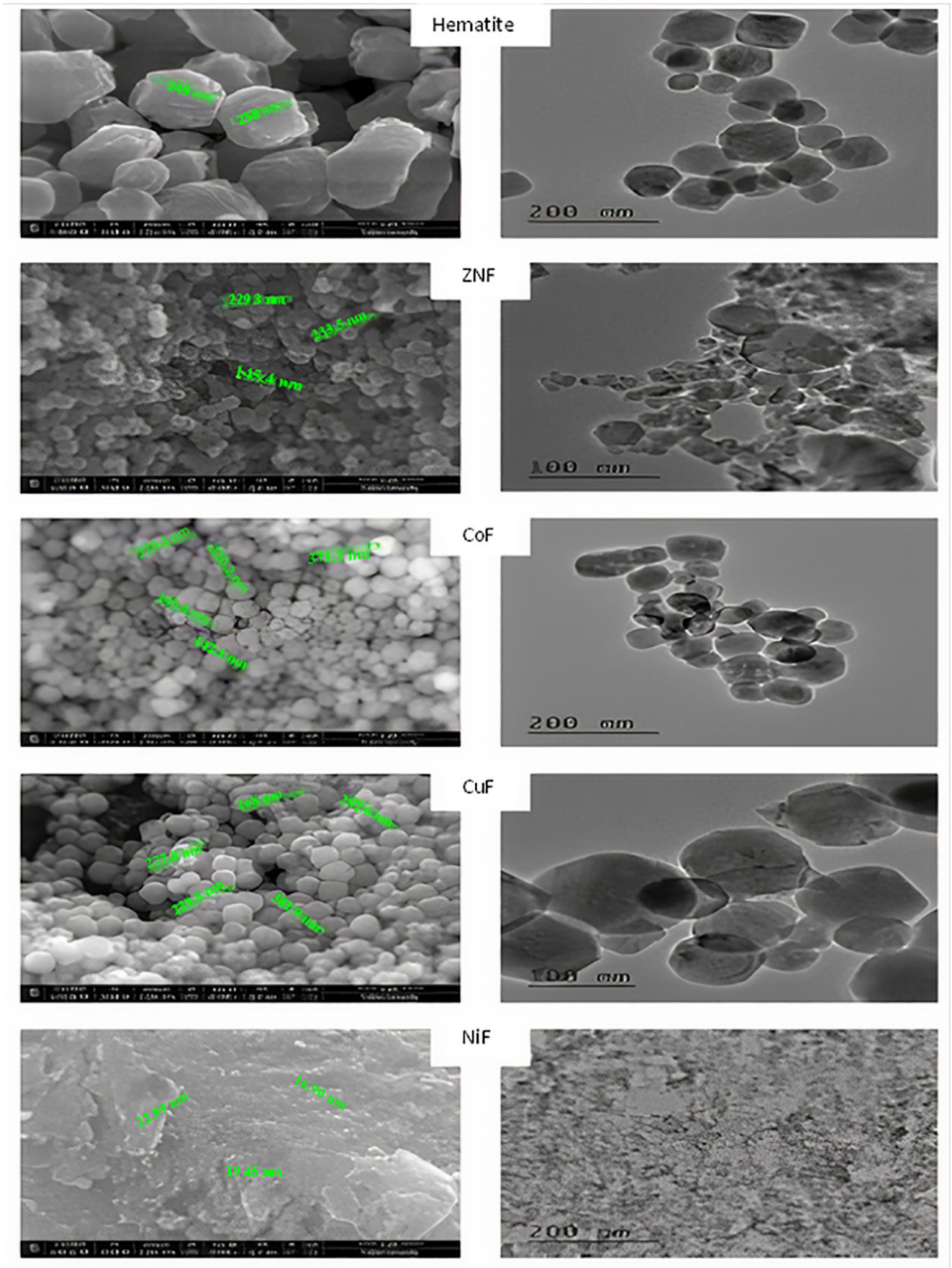

Fig. 2: SEM and TEM images of MFNPs, hematite; ZnF-NPs prepared with Zn salt; CoF-NPs prepared with Co salt; CuF-NPs prepared with Cu salt and NiF-NPs prepared with Ni salt

TABLE 1: VARIATION OF THE AREA OF DIFFERENT PEAKS OF ALBUMIN IN THE FTIR SPECTRA OF THE HUMAN SERUM ALBUMIN AND THEIR VARIATION AFTER CONTACT WITH DIFFERENT MFNPs (HEMATITE, ZnF: $ZnFe_2O_4$, CoF: $CoFe_2O_4$, NiF: $NiFe_2O_4$ and CuF: $CoFe_2O_4$) AND THE GRAIN SIZE

Samples	Albumin peak 2500-3800 cm^{-1}	Variation (%)	Grain size (nm)
Normal serum	128.3	-	-
Contact with ZnF	116.5	-9.2	212
Contact with CoF	120.6	-6	275
Contact with NiF	124.5	-2.9	56
Contact with CuF	124.3	-3.1	259
Contact with hematite	127	-1	1270

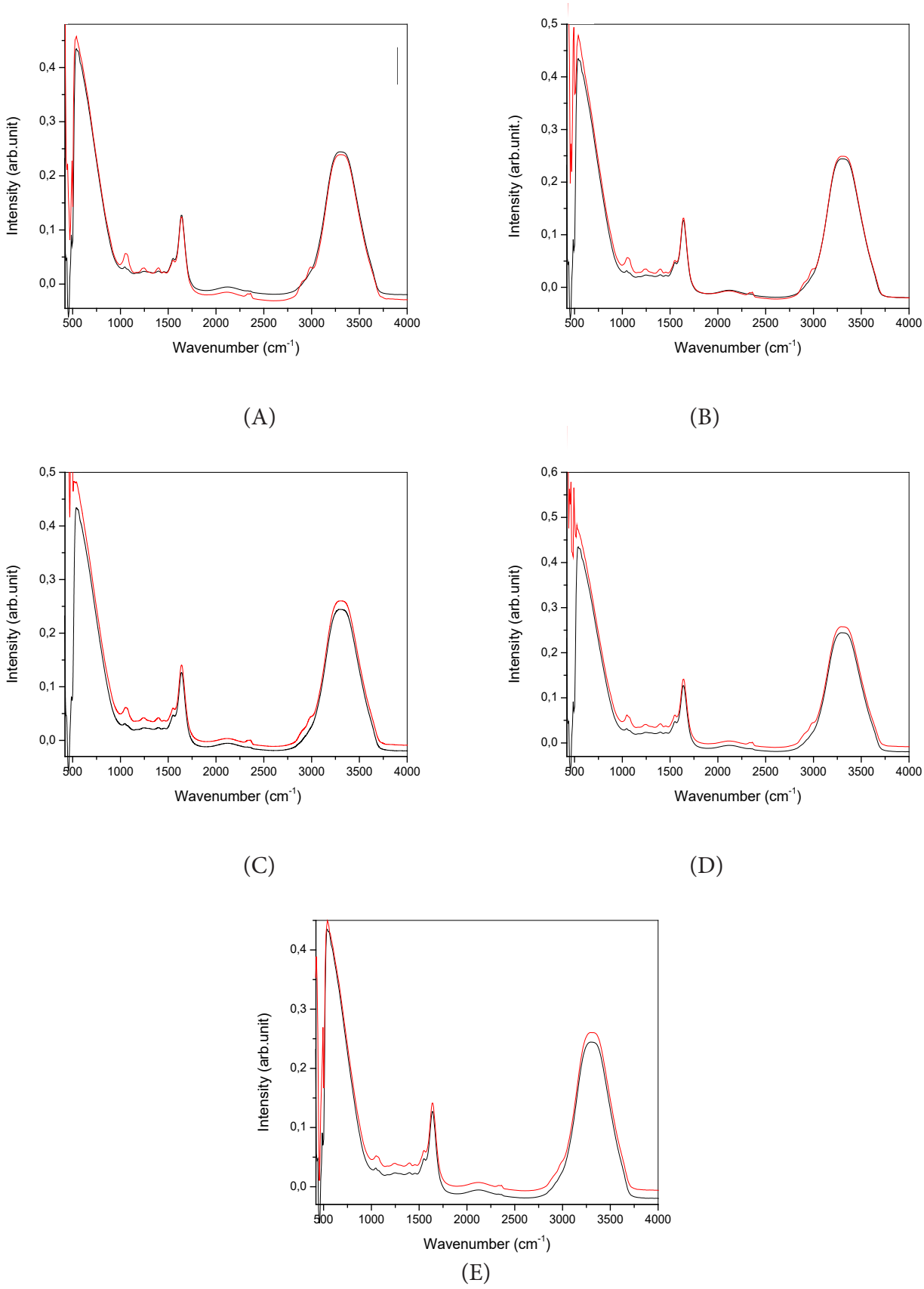

Fig. 3: FTIR absorption spectra of different MNFPs in the wavenumber range 1500-4000 cm^{-1}, (A) (—) Normal serum; (—) Contact with ZnF; (B) (—) Normal serum; (—) Contact with CoF; (C) (—) Normal serum; (—) Contact with $NiFe_2O_4$; (D) (—) Normal serum; (—) Contact with $CuFe_2O_4$ and (E) (—) Normal serum; (—) Contact with hematite

The wide absorption in the range of 2500-3100 cm^{-1} is due to the lipid content. Amides I and II are responsible for the absorption in the wave number range from 1400-1800 cm^{-1}, while the intense absorption in the band interval of 500-1400 cm^{-1} is assigned to the carbohydrates. As can be seen, the contact of serum with NPs caused a significant change in the FTIR spectra of the serum sample, indicating a modification in the serum composition. The effects of NPs contact are listed below for different regions.

For lipid region 2500-3100 cm^{-1}, the wide band located at the wavenumber range of 2800-3800 cm^{-1}, is assigned to lipids, which originated from N-H stretching vibration[33]. We noticed a reduction in the area of this peak because of nanopowder exposure (Table 1). This observed reduction was due to the reduction of the N-H bonding. The interaction of NPs with the serum component can take place through either the proteins adsorption or binding on the NP surface. The NPs are then coated by proteins, forming protein corona, which explain the reduction of the protein content in the solution.

Table 1 shows the reduction in the peak absorption and the NP grain size. Several researchers have claimed that the protein corona can be controlled by the size, shape and composition of the NPs[15,16,32,34-36]. In one study, Tenzer *et al.*[19] observed the formation of more than 166 protein corona using polystyrene and silica NPs of different sizes and charges[20].

Because the protein corona is formed by protein absorption on the nanopowder, the size of the produced protein corona is dependent on the specific area of the NPs and its size may be important. Reducing the particle grain size may enhance the protein-NP interaction surface. However, in our study, the lower grain size nano powders such as $NiFe_2O_4$ and hematite showed less effect than the larger grain size $ZnFe_2O_4$. This suggests that the protein affinity with NPs control the protein corona formation rather than grain size.

The contact with Zn ferrite resulted in a larger reduction in the protein content despite its large grain size. This suggests that Zn ferrite enjoys a higher affinity to protein than the other studied spinel ferrites, while the hematite has a lower effect, suggesting the low affinity of protein towards the hematite. It is worth mentioning here that Zn ions play a unique role in protein stabilization and in protein subunits folding through the Zn finger motifs[36] and in enzyme catalytic activity[34,35]. This explains the protein affinity to Zn and the formation of protein corona while using $ZnFe_2O_4$ NPs. Thereafter, Zn ferrite has been recommended as a medicine transporter compared with other studied NPs.

Nuclide acid region 1200-2000 cm^{-1} is the fingerprint of human albumin. There are two prominent amide absorption peaks located at 1655 cm^{-1} and 1546 cm^{-1} arising from C=O stretching and N-H vibration, termed amide I and amide II respectively. We noticed a stable absorption of amide I and amide II indicating that the studied NPs did not alter the amide structures.

Carbohydrate region 400-800 cm^{-1} is described here. In FTIR spectroscopy, we observed an increase in the area of the broad peak range of 400-800 cm^{-1}. This can be due to the formation of N-CO bonding. The protein corona formation, as deduced from the reduction of Infrared (IR) absorption in the range of 2550-3000 cm^{-1} can be followed by the breaking of bonds such as N-H, C-H present in the lipid[37]. Free Nitrogen (N) and Carbon (C) elements may interact to form new bonds such as N-CO and C-O, which are responsible for this peak enhancement (Table 1). As can be deduced from Table 1, $ZnFe_2O_4$ spinel ferrite has less effect on this serum component in contrast to $CuFe_2O_4$ and $NiFe_2O_4$ spinel ferrites.

The liberation of N and C might be responsible for the emergence of two new peaks located at 2350 and 3500 cm^{-1} and also to several other peaks. The enhanced peak is located at 1060.5 cm^{-1} that arises from C-O symmetric stretching of glucose. The peak at 1393.2 cm^{-1} is assigned to C=O symmetric stretching vibration of COO amino acid (fibrinogen) and the peak located at 1554.2 cm^{-1} is due to the N-H vibration of protein amine II[38].

Generally, the metal-oxide infrared vibration occurs at small wavenumbers. Several peaks appear in this region after contact with the NPs (fig. 4). The most interesting feature is that all used powders release atomic Fe in the solution, causing the formation of Fe-O, which is characterized by the peaks, located at 450 and 492 cm^{-1}. The divalent metal Ni (4893 cm^{-1} peak assigned to Ni-O vibration), Co (465 cm^{-1} due to Co-O vibration) and Cu (460.17 cm^{-1} and 495.06 cm^{-1} due to CuO) are also released from the nanopowder except Zn.

UV-visible spectroscopy analysis has been used by several authors for human blood serum and plasma characterization[39-41]. They suggested that the decrease in the UV-Visible absorbance at 280 nm

could be due to a change in the amino acid chain of the protein molecule, while the decrease in absorbance at the wavelength of 418 nm can be due to the blood constituent decrease of Co-hemoglobin. Fig. 5 shows the variation of UV-visible absorption spectra for the different NPs formulation at wavelength range from 220 to 700 nm. All the spectra peaks were found to be located at 280 and 417 nm. The strong peak at 280 nm, characteristic of the human blood serum, is due to the amide chain (amino acid: Tyrosine and tryptophan)[41]. This peak remained almost constant in different samples. This result is consistent with FTIR observations and confirms the stability of amide component in contact with NPs.

The peak located at 417 nm is assigned to the d-f transition of CO-oxyhemoglobin[42]. Gunasekaran *et al.* measured the 1.33 Optical Density (OD) of this peak in healthy serum and reported a reduction in OD in diseased individuals[41]. The contact with different NPs causes the reduction in OD at 417 from 1.9 to 1.02 as shown in fig. 6. The reduction in OD is a signature of the reduction of CO-oxyhemoglobin by adsorption on NPs. As shown, in fig. 6, the OD reduction follows the grain size variation. Lower grain size had a significant effect on OD, which suggests that the oxyhemoglobin was adsorbed on the NPs surface. It is worth noting that reducing the grain size increases both the specific surface of the NPs and increases its reactive surface.

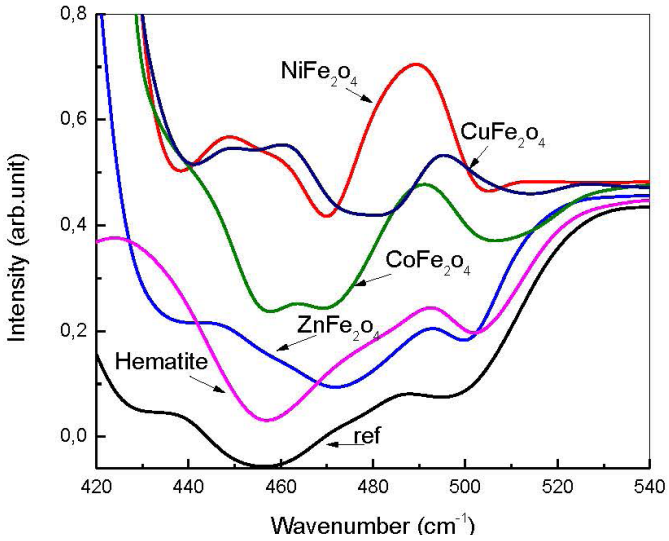

Fig. 4: FTIR absorption spectra of different MNFPs in the wavenumber range 400-500 cm^{-1}

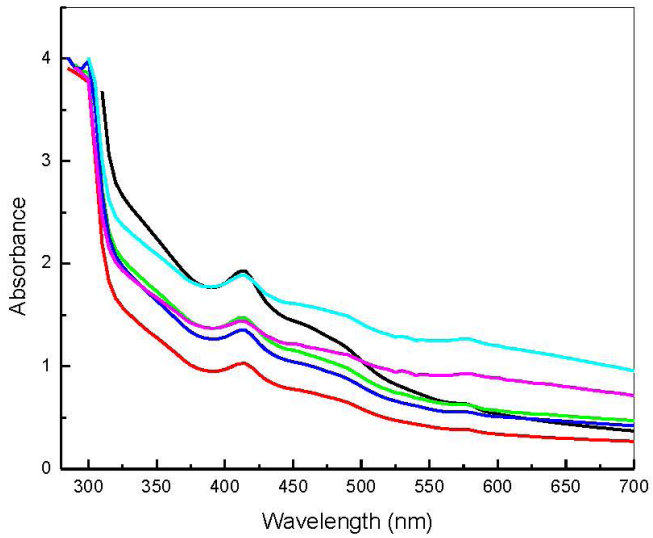

Fig. 5: UV-visible absorbance spectra of different MNFPs, (——) Ref; (——) Hematite; (——) $CuFe_2O_4$; (——) $NiFe_2O_4$; (——) $CoFe_2O_4$; (——) $ZnFe_2O_4$

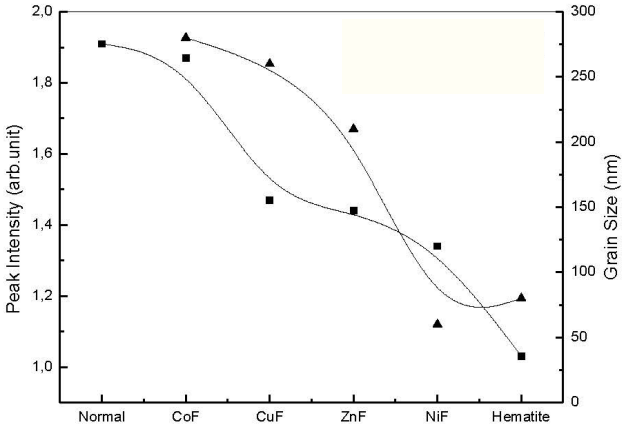

Fig. 6: Correlation between the peak intensity at the wavelength 417 nm with the grain size of different MFNPs, (—■—) Peak intensity; (—▲—) Grain size

From this study, it is quite clear that the formation of protein corona was controlled by the protein affinity towards the NPs rather than the grain size of the NPs. The amide composition of the serum was unaffected by the presence of NPs in contrast to the carbohydrate, which was found to be altered by NPs contact. A small amount of metallic oxide different metal was found to be released to the serum from the studied NPs. Due to its low effect on different serum component and the large affinity to protein spinel, Zn ferrite NPs have been recommended as the most suitable NP to be used for drug delivery.

Acknowledgements:

This study was funded by the Deputy of Scientific Research of King Abdulaziz University (Grant Number: G: 1577-141-1440). The authors gratefully acknowledge the technical and financial support of the Deanship of Scientific Research.

Conflict of interests:

The authors declared no conflict of interest.

REFERENCES

1. Yamashita F, Hashida M. Pharmacokinetic considerations for targeted drug delivery. Adv Drug Deliv Rev 2013;65(1):139-47.
2. Farokhzad OC, Langer R. Impact of nanotechnology on drug delivery. ACS Nano 2009;3(1):16-20.
3. Hafner A, Lovrić J, Lakoš GP, Pepić I. Nanotherapeutics in the EU: An overview on current state and future directions. Int J Nanomedicine 2014;9:1005.
4. Piazzini V, Landucci E, D'Ambrosio M, Fasiolo LT, Cinci L, Colombo G, *et al.* Chitosan coated human serum albumin nanoparticles: A promising strategy for nose-to-brain drug delivery. Int J Biol Macromol 2019;129:267-80.
5. El-Boubbou K. Magnetic iron oxide nanoparticles as drug carriers: Clinical relevance. Nanomedicine 2018;13(8):953-71.
6. Boateng-Marfo Y, Dong Y, Loh ZH, Lin H, Ng WK. Intravenous human serum albumin (HSA)-bound artemether nanoparticles for treatment of severe malaria. Colloids Surf A Physicochem Eng Asp 2018;536:20-9.
7. Choimet M, Hyoung-Mi K, Jae-Min O, Tourrette A, Drouet C. Nanomedicine: Interaction of biomimetic apatite colloidal nanoparticles with human blood components. Colloids Surf B Biointerfaces 2016;145:87-94.
8. Winzen S, Schoettler S, Baier G, Rosenauer C, Mailaender V, Landfester K, *et al.* Complementary analysis of the hard and soft protein corona: Sample preparation critically effects corona composition. Nanoscale 2015;7(7):2992-3001.
9. Del Pino P, Pelaz B, Zhang Q, Maffre P, Nienhaus GU, Parak WJ. Protein corona formation around nanoparticles-from the past to the future. Mater Horiz 2014;1(3):301-13.
10. Walkey CD, Chan WC. Understanding and controlling the interaction of nanomaterials with proteins in a physiological environment. Chem Soc Rev 2012;41(7):2780-99.
11. Khan MS, Tabrez S, Al-Okail MS, Shaik GM, Bhat SA, Rehman TM, *et al.* Non-enzymatic glycation of protein induces cancer cell proliferation and its inhibition by quercetin: Spectroscopic, cytotoxicity and molecular docking studies. J Biomol Struct Dyn 2021;39(3):777-86.
12. Monopoli MP, Åberg C, Salvati A, Dawson KA. Biomolecular coronas provide the biological identity of nanosized materials. Nat Nanotechnol 2012;7(12):779-86.
13. Martínez-Rodríguez NL, Tavárez S, González-Sánchez ZI. *In vitro* toxicity assessment of zinc and nickel ferrite nanoparticles in human erythrocytes and peripheral blood mononuclear cell. Toxicol *In Vitro* 2019;57:54-61.
14. Galdino FE, Picco AS, Sforca ML, Cardoso MB, Loh W. Effect of particle functionalization and solution properties on the adsorption of bovine serum albumin and lysozyme onto silica nanoparticles. Colloids Surf B Biointerfaces 2020;186:110677.
15. Givens BE, Xu Z, Fiegel J, Grassian VH. Bovine serum albumin adsorption on SiO_2 and TiO_2 nanoparticle surfaces at circumneutral and acidic pH: A tale of two nano-bio surface interactions. J Colloid Interface Sci 2017;493:334-41.
16. Givens BE, Wilson E, Fiegel J. The effect of salts in aqueous media on the formation of the BSA corona on SiO_2 nanoparticles. Colloids Surf B Biointerfaces 2019;179:374-81.

17. Monopoli MP, Walczyk D, Campbell A, Elia G, Lynch I, Baldelli Bombelli F, *et al.* Physical-chemical aspects of protein corona: Relevance to *in vitro* and *in vivo* biological impacts of nanoparticles. J Am Chem Soc 2011;133(8):2525-34.
18. Laurent S, Burtea C, Thirifays C, Rezaee F, Mahmoudi M. Significance of cell "observer" and protein source in nanobiosciences. J Colloid Interface Sci 2013;392:431-45.
19. Tenzer S, Docter D, Kuharev J, Musyanovych A, Fetz V, Hecht R, *et al.* Rapid formation of plasma protein corona critically affects nanoparticle pathophysiology. Nat Nanotechnol 2013;8(10):772-81.
20. Corbo C, Molinaro R, Tabatabaei M, Farokhzad OC, Mahmoudi M. Personalized protein corona on nanoparticles and its clinical implications. Biomater Sci 2017;5(3):378-87.
21. del Pilar Chantada-Vázquez M, López AC, Vence MG, Vázquez-Estévez S, Acea-Nebril B, Calatayud DG, *et al.* Proteomic investigation on bio-corona of Au, Ag and Fe nanoparticles for the discovery of triple negative breast cancer serum protein biomarkers. J Proteomics 2020;212:103581.
22. del Pilar Chantada-Vázquez M, López AC, Bravo SB, Vázquez-Estévez S, Acea-Nebril B, Núñez C. Proteomic analysis of the bio-corona formed on the surface of (Au, Ag, Pt)-nanoparticles in human serum. Colloids Surf B Biointerfaces 2019;177:141-8.
23. Hyder F, Manjura Hoque S. Brain tumor diagnostics and therapeutics with superparamagnetic ferrite nanoparticles. Contrast Media Mol Imaging 2017;2017.
24. Shah MR, Imran M, Ullah S. Nanocarriers for cancer diagnosis and targeted chemotherapy. Elsevier; 2019.
25. Angelova N, Yordanov G. Iron (III) and aluminium (III) based mixed nanostructured hydroxyphosphates as potential vaccine adjuvants: Preparation and physicochemical characterization. Colloids Surf A Physicochem Eng Asp 2017;535:184-93.
26. Gandhi S, Roy I. Synthesis and characterization of manganese ferrite nanoparticles, and its interaction with bovine serum albumin: A spectroscopic and molecular docking approach. J Mol Liq 2019;296:111871.
27. Akhavan O, Ghaderi E, Shahsavar M. Graphene nanogrids for selective and fast osteogenic differentiation of human mesenchymal stem cells. Carbon 2013;59:200-11.
28. Mahmoudi M, Lynch I, Ejtehadi MR, Monopoli MP, Bombelli FB, Laurent S. Protein-nanoparticle interactions: Opportunities and challenges. Chem Rev 2011;111(9):5610-37.
29. Caracciolo G. Liposome–protein corona in a physiological environment: Challenges and opportunities for targeted delivery of nanomedicines. Nanomedicine 2015;11(3):543-57.
30. Sakulkhu U, Maurizi L, Mahmoudi M, Motazacker M, Vries M, Gramoun A, *et al. Ex situ* evaluation of the composition of protein corona of intravenously injected superparamagnetic nanoparticles in rats. Nanoscale 2014;6(19):11439-50.
31. Ostroverkhov P, Semkina A, Nikitin A, Smirnov A, Vedenyapina D, Vlasova K, *et al.* Human serum albumin as an effective coating for hydrophobic photosensitizes immobilization on magnetic nanoparticles. J Magn Magn Mater 2019;475:108-14.
32. McUmber AC, Randolph TW, Schwartz DK. Electrostatic interactions influence protein adsorption (but not desorption) at the silica–aqueous interface. J Phys Chem Lett 2015;6(13):2583-7.
33. Barth A. The infrared absorption of amino acid side chains. Prog Biophys Mol Biol 2000;74(3):141-73.
34. Kumar S, Aswal VK, Callow P. pH-dependent interaction and resultant structures of silica nanoparticles and lysozyme protein. Langmuir 2014;30(6):1588-98.
35. Walkey CD, Olsen JB, Guo H, Emili A, Chan WC. Nanoparticle size and surface chemistry determine serum protein adsorption and macrophage uptake. J Am Chem Soc 2012;134(4):2139-47.
36. Brown RS, Sander C, Argos P. The primary structure of transcription factor TFIIIA has 12 consecutive repeats. FEBS Lett 1985;186(2):271-4.
37. Parraga G, Horvath SJ, Eisen A, Taylor WE, Hood L, Young ET, *et al.* Zinc-dependent structure of a single-finger domain of yeast ADR1. Science 1988;241(4872):1489-92.
38. Kluska K, Adamczyk J, Krężel A. Metal binding properties, stability and reactivity of zinc fingers. Coord Chem Rev 2018;367:18-64.
39. Gunasekaran S, Natarajan RK, Renganayaki V. UV visible spectrophotometric approach and absorption model for the discrimination of diseased blood. Asian J Chem 2008;20(1):48-54.
40. Haas SL, Müller R, Fernandes A, Dzeyk-Boycheva K, Würl S, Hohmann J, *et al.* Spectroscopic diagnosis of myocardial infarction and heart failure by Fourier transform infrared spectroscopy in serum samples. Appl Spectrosc 2010;64(3):262-7.
41. Gunasekaran S, Natarajan RK, Renganayaki V, Rathikha R. FTIR and UV visible spectrophotometric approach to discriminate leukemic sera. Asian J Chem 2008;20(4):2521-30.
42. Waterman MR. Methods in Enzymology. London-New York: Academic Press; 1955. p. 453.

This article was originally published in a special issue,"New Advancements in Biomedical and Pharmaceutical Sciences" Indian J Pharm Sci 2022:84(2) Spl Issue "191-199"